

Article

Capturing the Motion of Laser Pulse in Photoresist Mixture with Compressed Ultrafast Photography

Xinyue Liu ^{1,†}, Bin Xu ^{1,†}, Zihao Du ¹, Yi Ding ^{1,*}, Yi Hu ¹, Xiaojiang Zhan ¹, Shengbin Liao ² and Jiangtao Xi ³¹ Faculty of Intelligent Manufacturing, Wuyi University, Jiangmen 529020, China² National Engineering Research Center for E-Learning, Huazhong Normal University, Wuhan 430079, China³ School of Electrical, Computer and Telecommunications Engineering, University of Wollongong, Wollongong 2522, Australia

* Correspondence: dingyi1688@126.com

† These authors contributed equally to this work.

Abstract: Imaging the interaction between the laser pulse and photoresist mixture on the ultrafast time scale can track the path of the light pulse and reveal the procedure of the microstructure machining. However, most existing imaging technologies suffer from problems such as requiring multiple repeated shots or a limited time resolution. To overcome these problems, we propose to capture the motion of laser pulses in a photoresist mixture by using compressed ultrafast photography (CUP). In this method, we can recover the motion process of non-repeatable events with a single shot at the time-resolution of about 1.54×10^{11} fps, where the depth of the imaging sequence reaches hundreds of frames. To verify the effectiveness of the proposed method, we estimate the speed of the laser pulse in a photoresist mixture and evaluate the similarity between the image captured by a streak camera and our reconstructed ultrafast sequence; the results validate the reliability of our proposed method.

Keywords: ultrafast imaging; laser micromachining; compressed ultrafast photography

Citation: Liu, X.; Xu, B.; Du, Z.; Ding, Y.; Hu, Y.; Zhan, X.; Liao, S.; Xi, J. Capturing the Motion of Laser Pulse in Photoresist Mixture with Compressed Ultrafast Photography. *Photonics* **2022**, *9*, 903. <https://doi.org/10.3390/photonics9120903>

Received: 11 October 2022

Accepted: 23 November 2022

Published: 25 November 2022

Publisher's Note: MDPI stays neutral with regard to jurisdictional claims in published maps and institutional affiliations.



Copyright: © 2022 by the authors. Licensee MDPI, Basel, Switzerland. This article is an open access article distributed under the terms and conditions of the Creative Commons Attribution (CC BY) license (<https://creativecommons.org/licenses/by/4.0/>).

1. Introduction

The photoresist is a mixed liquid that contains a film-forming resin, photoreceptor, solvent, and other additives [1]. When the photoresist is exposed to the light source, such as a femtosecond laser, it undergoes a series of physical and chemical changes. The two-dimensional or three-dimensional microstructure can be fabricated by controlling the relative velocity of the focused laser beam and the photoresist. This approach has produced many precision components such as optical oscillators [2], micro grooves [3], Fresnel zone plate lens [4], and a micro lens [5]. If the interaction between the femtosecond pulse and the photoresist mixture could be visualized in a two-dimensional image sequence, it is possible to improve the accuracy of laser manufacturing [6].

Ultrafast imaging technologies have widely been used to capture various phenomena in materials science [7], plasma physics [8,9], nonlinear optics [10], cell biology [11], and other fields [12]. Due to the response speed limitations of electronic devices such as charge-coupled device (CCD) and a complementary metal oxide semiconductor (CMOS), the traditional electronic high-speed imaging technology for acquiring two-dimensional images has a speed limit of only 10^7 frames per second (fps) [13]. The ultrafast framing camera (UFC) has been demonstrated to capture 16 frames with an imaging speed of 3.33×10^8 fps [14]. The imaging speed of sequentially timed all-optical mapping photography (STAMP) can reach 4.4×10^{12} fps with six consecutive frames of imaging [15]. Its spectrally filtered variant version (SF-STAMP) captures the crystalline-to-amorphous phase transition of the $\text{Ge}_2\text{Sb}_2\text{Te}_5$ alloy with 25 frames at 7.52×10^{12} fps [16]. An important factor restricting its wide application is the limited number of imaging frames. The pump-probe technology is popular in capturing transient events [17]; it has also been used to observe

the femtosecond laser micromachining process. Wei et al. [18] used a time-resolved shadow graphic imaging system based on a femtosecond laser pump–probe to image the ultrafast process of the femtosecond laser ablating of micro-holes in silica glass. Bergner et al. [19] observed the energy deposition and subsequent relaxation processes after the interaction of the laser light with the glass material using pump–probe technology. Yu et al. [20] used pump–probe technology to observe the propagation of Bessel beams in poly methyl methacrylate (PMMA) and the resulting cylindrical pressure wave expansion. However, the phenomena captured by pump–probe technology should be reproducible [21]. In recent years, compressed ultrafast photography (CUP) has been developed to visualize many transient phenomena, including light propagation, reflection, refraction [22], optical Mach cone phenomenon [23], the dynamic process of optical soliton dissipation [24], and the spatiotemporal imaging of optical chaotic systems [25]. As an emerging ultrafast imaging method, CUP combines the feature of compressed sensing and the ultra-high temporal resolution of the streak camera, achieving the visualization of two-dimensional spatial information ultrafast imaging. The technology now has a temporal resolution higher than 10^{11} fps and a sequence depth of hundreds of frames [22]. Therefore, it is possible for CUP to capture the process of the interaction between the laser pulse and the photoresist mixture.

In this paper, we film the ultrafast laser pulse transmission process in a photoresist mixture with a streak camera and two-step iterative shrinkage/thresholding (TwIST) algorithm [26]. Meanwhile, to verify the reliability of the experimental results, we estimate the speed of the laser pulse in a photoresist mixture and evaluate the similarity between the image captured by the streak camera and our reconstructed ultrafast sequence with a peak signal-to-noise ratio (PSNR) and structure similarity index measure (SSIM) [27]. The results show that our method can capture the scattering motion process when the femtosecond laser pulse enters the photoresist mixture, which provides a potential approach to record the ultrafast process of laser machining.

The remaining sections of this paper are organized as follows. Section 2 presents the principles of CUP. Section 3 shows the experimental setup and results. Section 4 presents the discussion on our experimental results. Section 5 concludes the whole paper.

2. Principles

Figure 1 shows the original CUP system. The dynamic scene is first imaged from the lens to the intermediate image plane, then transferred to the digital micromirror device (DMD) by the $4f$ optical system, which consists of the tube lens and the objective lens [28]. During the operation, a pseudo-random binary mask image is created by pre-programmed switch duty cycle control. The DMD encodes two-dimensional ultrafast optical signals using the generated mask; the encoded signals are then transmitted into the streak camera with the completely opened slit by the $4f$ optical system. The encoded images are offset by the streak tube, and then these offsets are superimposed on the streak camera's internal CCD detector [29]. Currently, the streak camera records the result of the offset and superposition of the ultrafast optical signals in two-dimensional space at each moment. Based on the information recorded by the internal CCD detector, the compressive sensing image recovery algorithm is used to calculate and solve the two-dimensional ultrafast optical signals at each moment [30,31], thus the image sequence of ultrafast optical signals is formed. In this implementation process, CUP takes full advantage of the ultrafast imaging capability of the streak camera and the reconstruction capability of the compressed sensing algorithm.

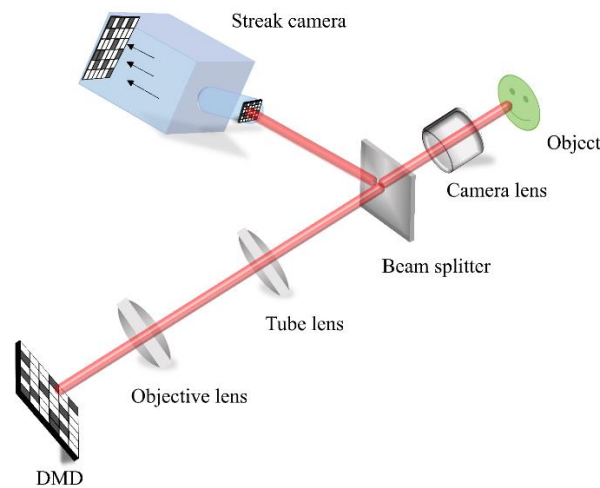


Figure 1. Schematic diagram of the original CUP system.

The forward model of CUP can be expressed as [22,23]:

$$E(m, n) = TSCI(x, y, t) \tag{1}$$

where $I(x, y, t)$ is the intensity distribution of the dynamic scene, T is the spatiotemporal integration operator, S is the temporal shearing operator, C is the encoding operator that comes from the DMD, and $E(m, n)$ is the observation image captured by the streak camera. Equation (1) shows that the three-dimensional dynamic scene $I(x, y, t)$ has been encoded into a two-dimensional image $E(m, n)$. To find the original image sequence frame, we should solve Equation (1). It is obvious that the number of elements in the 3D scene $I(x, y, t)$ is much larger than the number of elements in $E(m, n)$, so solving I is a process of solving an underdetermined system of equations. We can reconstruct sequential frames using compressed sensing algorithms because their principles are similar. In this paper, we adopt the TwIST algorithm to locate the minimal value of the following object function, as shown below:

$$\hat{I} = \underset{I}{\operatorname{argmin}} \left\{ 0.5 \|E(m, n) - TSCI(x, y, t)\|_2^2 + \tau \Phi[I(x, y, t)] \right\} \tag{2}$$

where $\|\cdot\|_2$ is the l_2 norm and τ is the regularization parameter. $\Phi(X)$ is the regularization function to encourage sparsity in the spatial gradient domain. In Equation (2), the first term $\|E(m, n) - TSCI(x, y, t)\|_2^2$ is minimized when the actual measurement E closely matches the predicted solution, and $TSCI$, the second term, $\Phi(I)$ encourages I to be a piecewise constant (i.e., sparse in the spatial gradient domain). The weights of these two terms adjusted by τ lead to the results that are most consistent with the ground truth. $\Phi(X)$ can be written as:

$$\begin{aligned} \Phi(X) = & \sum_{k=1}^{N_z} \sum_{i=1}^{N_x \times N_y} \sqrt{(\Delta_i^h X_k)^2 + (\Delta_i^v X_k)^2} \\ & + \sum_{m=1}^{N_y} \sum_{i=1}^{N_x \times N_z} \sqrt{(\Delta_i^h X_m)^2 + (\Delta_i^v X_m)^2} \\ & + \sum_{n=1}^{N_x} \sum_{i=1}^{N_y \times N_z} \sqrt{(\Delta_i^h X_n)^2 + (\Delta_i^v X_n)^2} \end{aligned} \tag{3}$$

where N_x and N_y are the row and column pixel numbers in each image; N_z is the image number; $k, m,$ and n are the indices; $X_k, X_m,$ and X_n represent the 2D datum along the indices $k, m,$ and $n,$ respectively; and Δ_i^h, Δ_i^v are the horizontal and vertical first-order local difference operators on the 2D datum.

When reconstructing a dynamic scene $I(x, y, t)$ with $N_x \times N_y \times N_t$ dimensions, $N_x, N_y,$ and N_t represent the number of voxels along $x, y,$ and $t,$ respectively. The dimension of the mask $C_{x,y}$ displayed by DMD is $N_x \times N_y$. After the clipping and superposition of the streak camera, the actual spatial dimension of the mask $C_{x,y-t}$ will be supplemented

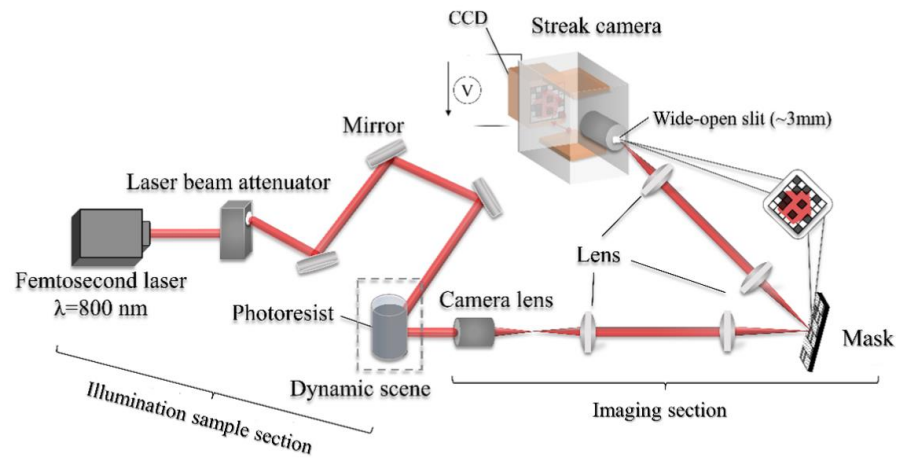
by zero to $N_x \times (N_y + N_t - 1)$, and the actual spatial dimension of the three-dimensional dimension $I_{x,y-t,t}$ at the imaging location is zero-filled to $N_x \times (N_y + N_t - 1) \times N_t$.

To verify the effectiveness of our experimental method, we also compare the PSNR and SSIM of $E(m, n)$ and $E'(m, n)$ in Section 3. $E(m, n)$ is the image captured by the streak camera, $E'(m, n)$ is the image generated by encoding and compressing the reconstructed ultrafast images $I(x, y, t)$ according to the CUP imaging principle.

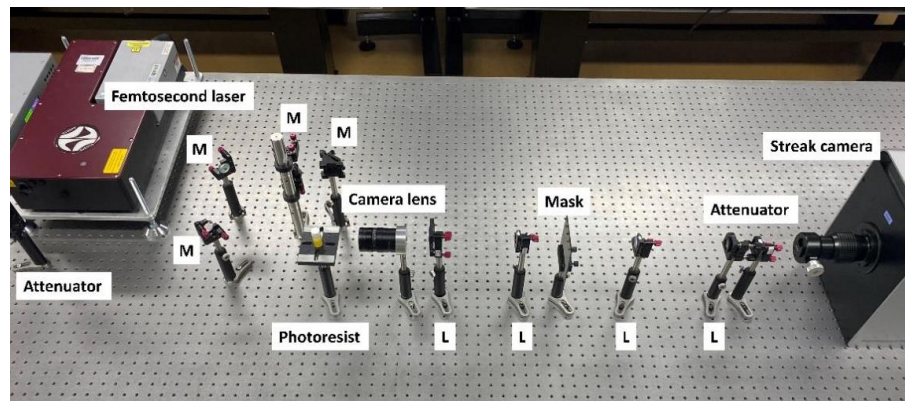
3. Experiments and Results Analysis

3.1. Experimental Setup and Results

The schematic diagram of the experimental system built in this paper is shown in Figure 2a. The 800 nm femtosecond laser (AVESTA/ TIF-SP-30-F10) generates a light pulse of 30 fs with a power of around 1000 mw. If the energy of the light pulse is high, shooting dynamic scenes will result in an overexposure, which will damage the streak camera, so we use a laser beam attenuator (ATT30, Thorlabs, Newton, NJ, USA) to reduce the light intensity. The laser beam is collimated and adjusted to the same height as the streak camera using three mirrors. When the light pulse enters the photoresist mixture, the dynamic scene is captured by the camera lens (CF75HA-1, Fujinon, Wayne, NJ, USA) and passes through the first optical 4f system (AC254-075-A, Thorlabs; AC254-100-A, Thorlabs) before reaching the mask board, where a pseudo-random binary pattern is inscribed to encode the scene. The image carrying the encoded information is then passed through the second optical 4f system (AC254-100-A, Thorlabs; AC254-150-A, Thorlabs) and into the streak camera (Model 2200, XIOPM, Xi'an, China) with the slit fully open. Finally, a compressed image is captured by the CCD inside the streak camera.



(a)



(b)

Figure 2. Experimental setup. (a) Experimental arrangement for observing the motion of light pulse in photoresist mixture with CUP system. (b) Actual optical path.

It is worth noting that compared to the original CUP system shown in Figure 1, we replaced the DMD with a mask board, which is engraved with a pre-programmed coding matrix. The mask board is used to facilitate the construction of the light path and reduce the mixed invalid coding information in the observed image. We also split the same optical $4f$ system in the original CUP optical path into two different $4f$ systems for three purposes: (1) since the size of the mask board is large, we magnify the ultrafast dynamic scene with the first $4f$ system to fully illuminate the mask board for an effective image coding, and (2) the encoded ultrafast dynamic scene is magnified by the second $4f$ system, which helps to focus the image in light path adjustment. (3) After splitting the $4f$ system, it is not necessary to use a beam splitter, which can effectively enhance the light intensity of the optical signal and improve the contrast of the image. This design has positive impacts in establishing a CUP system with a low intensity light source, which facilitates the streak camera to capture clear images more easily. Figure 2b shows the actual optical path of our experiment.

In our experiment, the scanning level of the streak camera is 125 ps [32], so the temporal resolution of the streak camera is about 0.06 ps/pixel. Meanwhile, the shearing velocity of the streak camera is set to $v = 20$ mm/ns. Additionally, the internal CCD size of the streak camera is 1024×1024 pixels (2×2 binning; binned pixel size $d = 13$ μm). Therefore, the reconstructed frame rate, v' , is determined by $v' = v/d$ to be 1.538×10^{11} fps [22].

We use AZ[®] nLOF[™] 2000 Series I-line photoresist in the experiment [33]. The experimental samples are the photoresist without water and the photoresist mixed with water at a 1:3 and 1:1 volume ratio, respectively. Three experimental samples are prepared at the same stirring frequency and time.

Before the experiment, a background image of the streak camera is taken with the slit completely opened to reduce the influence of noise in image reconstruction (see Figure 3a). Meanwhile, the pseudo-random binary pattern generated by the mask board is photographed, as shown in Figure 3b. After that, the laser is turned on and the light pulse enters the photoresist mixture. The dynamic scene is captured by the streak camera and three compressed scene images are obtained, as shown in Figure 3c–e. Figure 3c corresponds to the case that the femtosecond laser enters the photoresist mixed with water at 1:3; Figure 3d corresponds to the case that the femtosecond laser enters the photoresist mixed with water at 1:1 and Figure 3e corresponds to the case that the femtosecond laser enters the photoresist without water.

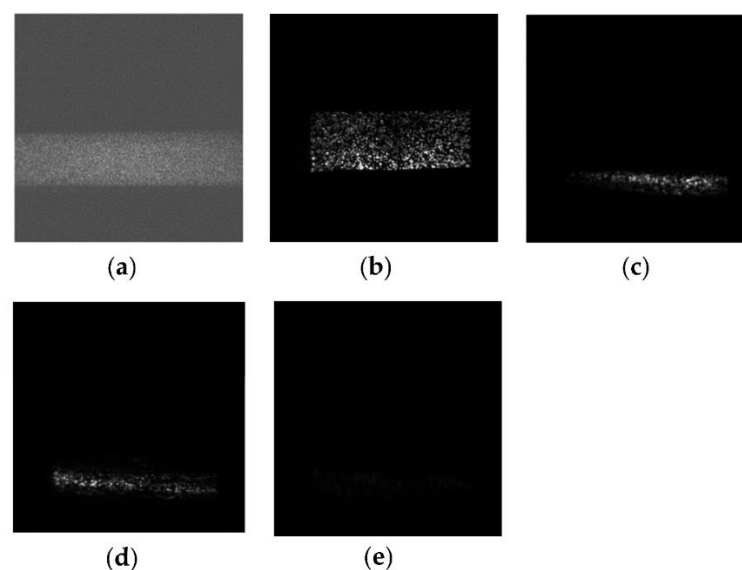
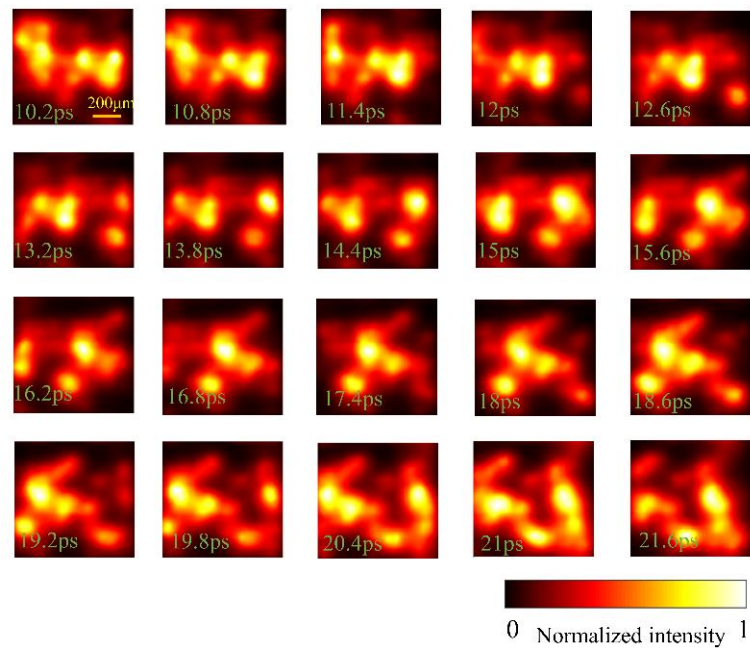
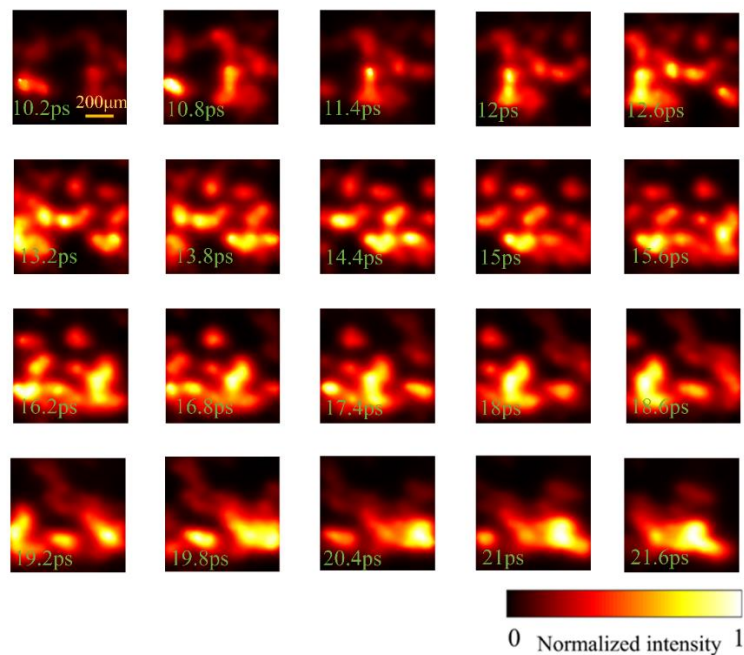


Figure 3. Images taken by the streak camera: (a) background image. (b) Pattern image. (c) Observed image (photoresist: water = 1:3 volume ratio). (d) Observed image (the volume ratio of photoresist: water = 1:1 volume ratio). (e) Observed image (without water addition).

The captured background image, mask image, and scene images are put into Equation (2), then the transient sequence of ultrafast laser motion is solved with the TwIST algorithm. To illustrate the moving process of the laser scattering, we select the reconstruction results of the pixels from the 1300th row to the 1700th row in Figure 3c–e; the spatial resolution of the reconstructed images is 128×527 . After processing, 400 frames of images can be reconstructed within 20 min. We select some representative frames to show in Figure 4. Figure 4a shows the reconstructed results when the ratio of the photoresist concentration to water is 1:3, Figure 4b shows the reconstructed results when the ratio of photoresist concentration to water is 1:1, and Figure 4c shows the reconstructed results of photoresist without water.



(a)



(b)

Figure 4. Cont.

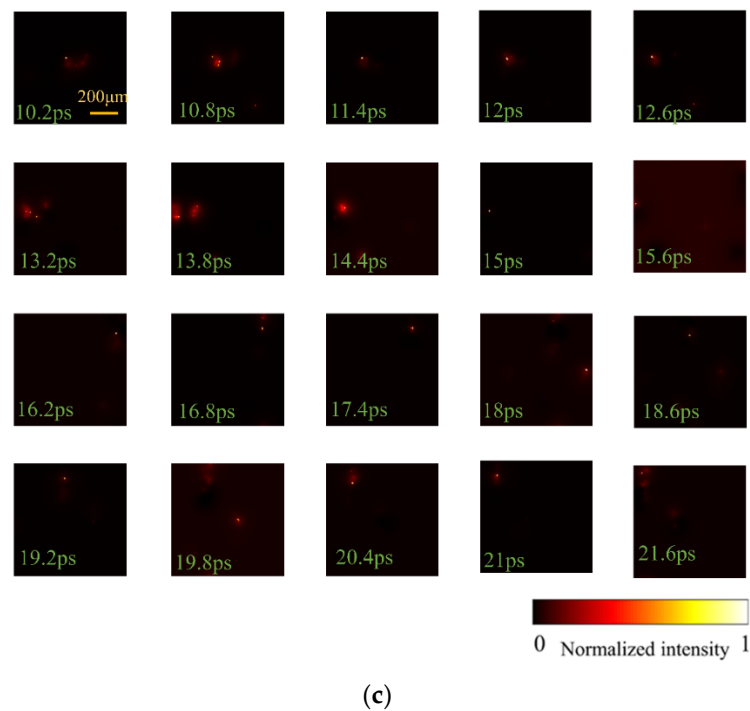


Figure 4. Representative frames of reconstruction results. (a) Reconstructed images (the volume ratio of photoresist: water = 1:3 volume ratio). (b) Reconstructed images (the volume ratio of photoresist: water = 1:1 volume ratio). (c) Reconstructed images photoresist (without water addition).

From Figure 4, we can see that the scattering intensity of the photoresist mixture with different water concentrations is different. Figure 4a,b shows that the scattering intensity of the photoresist mixture with a higher water concentration is larger than the photoresist mixture with a lower water concentration. Figure 4c shows that it is difficult to observe the scattering of a light pulse in the photoresist without water. We also calculate the average lightness (AL) values of Figure 4a–c. The calculation formula of the AL is as follows:

$$AL = \frac{1}{M \times N} \sum_{x=0}^{M-1} \sum_{y=0}^{N-1} L(x, y) \tag{4}$$

where M and N represent the row and column of the image, respectively. $L(x, y)$ represents the lightness of each pixel point. The average lightness of Figure 4a–c is 51.6, 44.2, and 2.2, respectively. Based on this result, we speculate that under the condition of a certain light intensity, the scattering intensity of the light pulse may be related to the concentration of water in the photoresist mixture.

3.2. Analysis

To verify the accuracy of the reconstructed results, we calculate the velocity of the laser pulse from the reconstructed images in Figure 4a. The refractive index of the experimental sample (mixture of photoresist and water) ranges from 1.3 to 1.6 (1.3 in water and 1.6 in photoresist). Therefore, the theoretical value of the speed of light in the photoresist mixture is between 1.87×10^8 m/s and 2.30×10^8 m/s.

As shown in Figure 5, we label one light pulse from the reconstructed ultrafast images with the green grid. From these images, we can see that the spatial location of the light pulse is time-varying, and the velocity of the light pulse could be inferred with the changes in the spatial location and the time interval between the images. For example, from the reconstructed frame at 12.6 ps to the reconstructed frame at 13.8 ps (20 frames are included), the light pulse moves about 20 pixels (single pixel size occupies 6.5 μm). Meanwhile, as

the shearing effect of the streak camera, the light pulse in fact moves by 20 pixels, thus the light pulse moves by $(20 + 20) \times 6.5 \mu\text{m} = 260 \mu\text{m}$ in total within 1.2 ps.

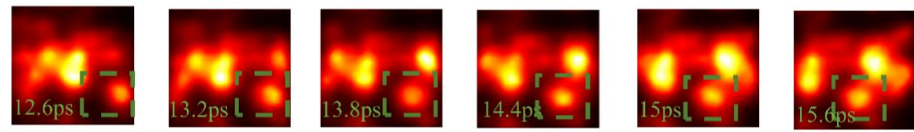


Figure 5. Images of tracking photon centroid.

Therefore, we obtain the velocity of the laser pulse results shown in Figure 6. The light speed in the photoresist mixture recovered by our proposed method is $(2.1 \pm 0.2) \times 10^8 \text{ m/s}$; this result is consistent with the theoretical range (between $1.87 \times 10^8 \text{ m/s}$ and $2.30 \times 10^8 \text{ m/s}$). Thus, we can conclude that the reconstruction results of our proposed method are reasonable.

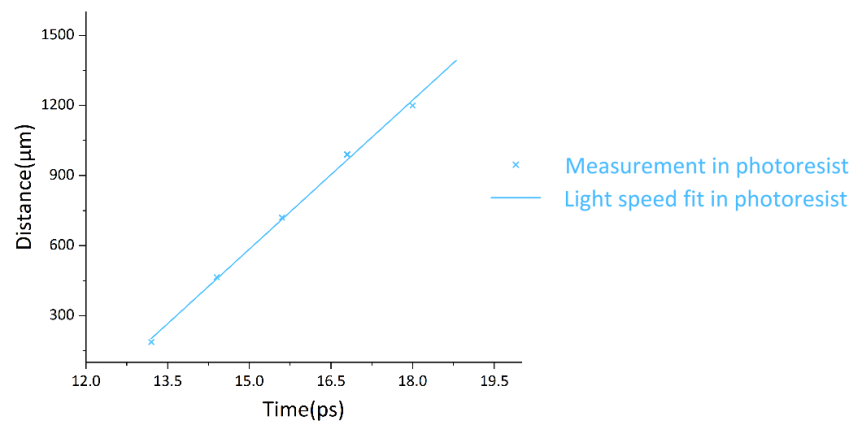


Figure 6. Recovered light speed in photoresist mixture.

On the other hand, to validate the reliability of our proposed method, we also evaluate the similarity between the image captured by the streak camera $E(x, y)$ and our reconstructed ultrafast sequence $I(x, y, t)$ in the case of photoresist mixed with water at 1:3. In this procedure, we code the reconstructed sequence frames $I(x, y, t)$ into a new image $E'(x, y)$ according to the compressed ultrafast imaging principle; the PSNR and SSIM of $E(x, y)$ and $E'(x, y)$ are calculated to verify the reliability of the experimental results. This validation process of our experiment can be summarized in three steps, as shown in Figure 7.

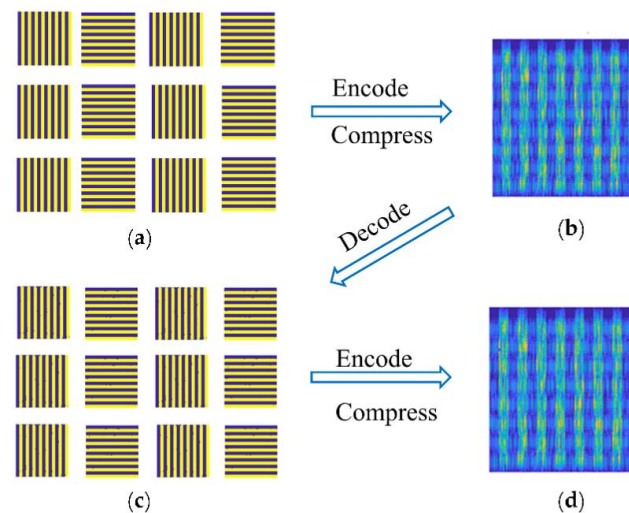


Figure 7. The whole process of our experiment: (a) original image sequence frames; (b) encoded and compressed $E(m, n)$; (c) reconstructed images; (d) encoded and compressed $E'(m, n)$.

1. The first step is to capture the ultrafast dynamic scene with the compressed ultrafast imaging system. The ultrafast scene images are encoded, compressed, and superimposed into the streak camera; the captured image of the streak camera is $E(m, n)$, as shown in Figure 7b.
2. In the second step, a series of reconstructed images $I(x, y, t)$ are obtained by using the TwIST algorithm, as shown in Figure 7c.
3. In the third step, the reconstructed images $I(x, y, t)$ are encoded and compressed according to the compressed ultrafast imaging principle to obtain image $E'(m, n)$, as shown in Figure 7d. Then, we calculate the PSNR [34] and SSIM [35] of $E(m, n)$ and $E'(m, n)$ to verify the reliability of our proposed method.

The PSNR and SSIM are important criteria for the objective evaluation of the image quality. The calculation formula of the PSNR is as follows:

$$\text{MSE} = \frac{1}{H \times W} \sum_{i=1}^H \sum_{j=1}^W (X(i, j) - Y(i, j))^2 \tag{5}$$

$$\text{PSNR} = 10 \log_{10} \left(\frac{(2^N - 1)^2}{\text{MSE}} \right) \tag{6}$$

where the mean square error (MSE) represents the mean square error of the current image X and the reference image Y , H , and W are the height and width of the image, respectively. N is the number of bits per pixel, of which the general value is eight.

The calculation formula of SSIM is given by:

$$\text{SSIM}(X, Y) = \frac{(2\mu_x\mu_y + C_1)(2\sigma_{xy} + C_2)}{(\mu_x^2 + \mu_y^2 + C_1)(\sigma_x^2 + \sigma_y^2 + C_2)} \tag{7}$$

where $\mu_x, \mu_y, \sigma_x, \sigma_y$, and σ_{xy} are the local mean, standard deviation, and cross-covariance of image X and Y , C_1, C_2 , and C_3 are the regularization constants of the brightness, contrast, and structurization, respectively.

It should be noted that the reconstruction process is the optimization process of objective function \hat{I} based on Equation (2), which is an ill-conditioned equation with far more unknowns than the equations. In other words, as the number of reconstructed images increases, the unknown quantity will also change significantly, and the error will fluctuate accordingly. Therefore, it is of great significance to study the frame number of the reconstructed images for the parameter selection of the experiment. To this end, we reconstruct the transient process with a different number of images (i.e., the sequences with different time intervals), including 10, 20, . . . 400 frames. In all cases, we calculate the PSNR and SSIM in relation to the image captured by the streak camera. The result is shown in Figure 8.

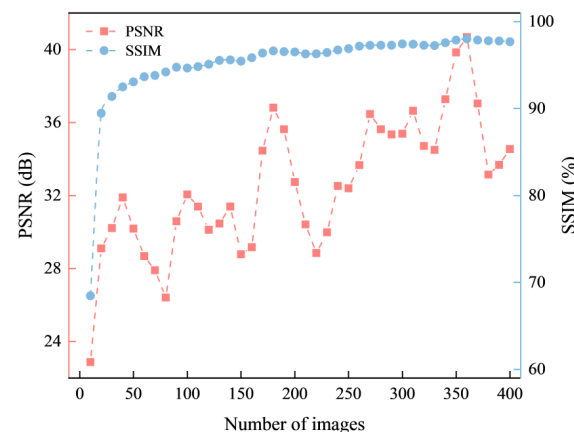


Figure 8. PSNR and SSIM indexes.

In Figure 8, the red dots are the PSNR results, the blue dots are the SSIM results, and the horizontal axis represents the number of reconstructed images. The highest value of the PSNR is 40.6796 dB and the lowest is 22.8753 dB, with an average of 32.5888 dB. Although there is an obvious decrease in the PSNR value from the 50th to the 80th frame and the 170th to 220th frame, the PSNR value still remains above 28.8455 dB. The highest SSIM is 98.02%, the lowest is 68.46%, and the average value is 95.25%. The lowest SSIM value is at the 10th frame, which increases to 89.46% at the 20th frame and is more than 91.40% from the 30th frame. It can be seen that the SSIM value does not change much when the number of image reconstruction frames reaches 200. The PSNR value fluctuates greatly with the number of the image, which may result from the change in the weight factor τ in Equation (2). The existing best results of PSNR and SSIM are obtained when the number of frames reaches 350. In future research, we will investigate the influence of the number of frames and other parameters to find the best PSNR and SSIM.

According to our reconstructed ultrafast sequence, the velocity of the light pulse in the photoresist mixture fell within the reasonable range, and the PSNR and SSIM values also demonstrate a high quality. Therefore, we can conclude that the reconstructed sequence reflects the transient process of the optical pulse movement inside the photoresist mixture, which verifies the feasibility and reliability of our proposed method.

4. Discussion

The existing TwIST algorithm can effectively reconstruct compressed images captured by the streak camera, but its high computation amount still limits its application. It takes about 20 min for reconstructing 400 images with the size of 128×527 pixels in this paper. The time-consuming steps are mainly in the iteration process. Each iteration of the algorithm uses the previous two iteration values and the denoising operator to update the current value. We think the speed of the calculation can be accelerated by using specially designed hardware such as GPU or FPGA. Meanwhile, the reconstruction quality of the images varies with the value of the weight factor τ in the TwIST algorithm. As shown in Figure 8, with the increase in the number of images, the value of PSNR is obviously changed. We believe that machine learning may be used to search the weight factor τ to obtain higher quality reconstructed images. The encoding pattern also has a great influence on the running time of the algorithm and the quality of the reconstructed image. Although a random encoding matrix is used in this paper, it may not be the best choice for some ultrafast scenarios. For example, for the dynamic scene with known prior conditions (such as fringe images), it can be encoded by designing a specific pattern, which can improve the reconstruction speed and quality; for dynamic scenes without a priori conditions, the dynamic scene can be divided into multiple replicas in space, then each replica passes through a different random encoding region, and finally all these encoded replicas are sent to a streak camera for imaging. If the speed and quality of CUP are improved to achieve a real-time, fast, high-quality image reconstruction, it could be used in observing and researching more ultrafast phenomena in biomedical and materials processing.

5. Conclusions

In this paper, we capture the propagation process of the ultrafast laser pulse in a photoresist mixture by using the improved CUP system. In the experiment, two optical 4f systems are used to reduce the optical signal loss as much as possible and improve the image signal-to-noise ratio. The scattering intensity in the photoresist mixture is observed and, according to the reconstructed ultrafast sequences, we infer that the intensity of the scattering may be related to the concentration of water in the photoresist mixture. To validate the effectiveness of our proposed method, we estimate the speed of the laser pulse in a photoresist mixture based on the reconstructed image sequence, and the results show that the speed of the laser pulse falls within a reasonable range. We also evaluate the similarity between the image captured by the streak camera and our reconstructed ultrafast sequence to verify the effectiveness of our proposed method. The results show that with

the increase in the number of reconstructed images, the quality of the reconstructed signals keeps rising on a high level, indicating that our CUP system is capable of two-dimensional ultrafast imaging. From these results, we can conclude that the method proposed in this paper provides a possible approach to capture the transient phenomena in ultrafast laser machining.

Author Contributions: Conceptualization, X.L., B.X. and Y.D.; methodology, X.L., B.X. and Y.D.; software, Z.D. and X.Z.; validation, B.X., X.L. and Y.H.; formal analysis, X.Z., Y.D., B.X., Z.D., S.L. and J.X.; investigation, X.Z., B.X. and S.L.; resources, Y.D., Y.H. and J.X.; data curation, B.X. and X.L.; writing—original draft preparation, B.X. and X.L.; writing—review and editing, B.X. and Y.D.; visualization, X.L. and Y.D.; supervision, Y.D. and Y.H.; project administration, Y.D.; funding acquisition, Y.D. and J.X. All authors have read and agreed to the published version of the manuscript.

Funding: This work was supported by the National Natural Science Foundation of China (Grant No. 62075168), (Grant No. 62077023) and the Key Scientific Research Platforms and Projects of Ordinary Universities in Guangdong Province (Grant No. 2021KCXTD051).

Institutional Review Board Statement: Not applicable.

Informed Consent Statement: Not applicable.

Data Availability Statement: The data presented in this study are available on reasonable request from the corresponding author.

Conflicts of Interest: The authors declare no conflict of interest.

References

1. Dill, F.H.; Hornberger, W.P.; Hauge, P.S.; Shaw, J.M. Characterization of positive photoresist. *IEEE Trans. Electron. Devices* **1975**, *22*, 445–452. [[CrossRef](#)]
2. Kowalewicz, A.; Sharma, V.; Ippen, E.; Fujimoto, J.G.; Minoshima, K. Three-dimensional photonic devices fabricated in glass by use of a femtosecond laser oscillator. *Opt. Lett.* **2005**, *30*, 1060–1062. [[CrossRef](#)] [[PubMed](#)]
3. Borowiec, A.; Haugen, H.K. Femtosecond laser micromachining of grooves in indium phosphide. *Appl. Phys. A* **2004**, *79*, 521–529. [[CrossRef](#)]
4. Sohn, I.-B.; Ahsan, M.S.; Noh, Y.-C.; Choi, H.-K.; Kim, J.-T.; Ko, M.J. Fabrication of Fresnel zone plate lens in fused silica glass using femtosecond laser lithography technology. *Opt. Eng.* **2014**, *53*, 55107. [[CrossRef](#)]
5. Wu, D.; Wu, S.-Z.; Niu, L.-G.; Chen, Q.-D.; Wang, R.; Song, J.-F.; Fang, H.-H.; Sun, H.-B. High numerical aperture microlens arrays of close packing. *Appl. Phys. Lett.* **2010**, *97*, 31109. [[CrossRef](#)]
6. Liang, Y.; Zhou, J.; Yin, D.; Zheng, Y.; Qi, H.; Wang, M.; Cheng, Y. Monolithically integrated electro-optic modulator fabricated on lithium niobate on insulator by photolithography assisted chemo-mechanical etching. *J. Phys. Photonics* **2021**, *3*, 34019. [[CrossRef](#)]
7. Sakakura, M.; Terazima, M.; Shimotsuma, Y.; Miura, K.; Hirao, K. Observation of pressure wave generated by focusing a femtosecond laser pulse inside a glass. *Opt. Express* **2007**, *15*, 5674–5686. [[CrossRef](#)]
8. Wei, Y.; Li, B.; Wei, X.; Yu, Y.; Wong, K.K.Y. Ultrafast spectral dynamics of dual-color-soliton intracavity collision in a mode-locked fiber laser. *Appl. Phys. Lett.* **2018**, *112*, 81104. [[CrossRef](#)]
9. Šiaulyys, N.; Melninkaitis, A.; Dubietis, A. In situ study of two interacting femtosecond filaments in sapphire. *Opt. Lett.* **2015**, *4*, 2285–2288. [[CrossRef](#)]
10. Geints, Y.E.; Minina, O.V.; Geints, I.Y.; Seleznev, L.V.; Pushkarev, D.V.; Mokrousova, D.V.; Rizaev, G.E.; Shipilo, D.E.; Nikolaeva, I.A.; Kurilova, M.V.; et al. Nonlinear Propagation and Filamentation on 100 Meter Air Path of Femtosecond Beam Partitioned by Wire Mesh. *Sensors* **2022**, *22*, 6322. [[CrossRef](#)]
11. Lei, C.; Kobayashi, H.; Wu, Y.; Li, M.; Isozaki, A.; Yasumoto, A.; Mikami, H.; Ito, T.; Nitta, N.; Sugimura, T. High-throughput imaging flow cytometry by optofluidic time-stretch microscopy. *Nat. Protoc.* **2018**, *13*, 1603–1631. [[CrossRef](#)] [[PubMed](#)]
12. Kudryashov, S.I.; Seleznev, L.V.; Rudenko, A.A.; Ionin, A.A. In situ supercontinuum nanopatterning of silicon surface by femtosecond laser super-filaments. *JETP Lett.* **2019**, *109*, 157–162. [[CrossRef](#)]
13. Etoh, T.G.; Vo Le, C.; Hashishin, Y.; Otsuka, N.; Takehara, K.; Ohtake, H.; Hayashida, T.; Maruyama, H. Evolution of ultra-high-speed CCD imagers. *Plasma Fusion Res.* **2007**, *2*, S1021. [[CrossRef](#)]
14. Tiwari, V.; Sutton, M.; McNeill, S.R. Assessment of high speed imaging systems for 2D and 3D deformation measurements: Methodology development and validation. *Exp. Mech.* **2007**, *47*, 561–579. [[CrossRef](#)]
15. Nakagawa, K.; Iwasaki, A.; Oishi, Y.; Hirosaki, R.; Tsukamoto, A.; Hirosawa, K.; Liao, H.; Ushida, T.; Goda, K.; Kannari, K. Sequentially timed all-optical mapping photography (STAMP). *Nat. Photonics* **2014**, *8*, 695–700. [[CrossRef](#)]
16. Suzuki, T.; Hida, R.; Yamaguchi, Y.; Nakagawa, K.; Saiki, T.; Kannari, F. Single-shot 25-frame burst imaging of ultrafast phase transition of Ge₂Sb₂Te₅ with a sub-picosecond resolution. *Appl. Phys. Express* **2017**, *10*, 92502. [[CrossRef](#)]

17. Domke, M.; Rapp, S.; Schmidt, M.; Huber, H.P. Ultrafast pump-probe microscopy with high temporal dynamic range. *Opt. Express* **2012**, *20*, 10330–10338. [[CrossRef](#)]
18. Wei, J.; Zhang, B.; Liu, H.; Zhang, H. Time-Resolved Shadowgraphic Imaging of Femtosecond Laser Ablated Micro-Holes in Silica Glass. *Chin. J. Lasers* **2019**, *46*, 508020.
19. Bergner, K.; Seyfarth, B.; Lammers, K.A.; Ullsperger, T.; Döring, S.; Heinrich, M.; Kumkar, M.; Flamm, D.; Tünnermann, A.; Nolte, S. Spatio-temporal analysis of glass volume processing using ultrashort laser pulses. *Appl. Opt.* **2018**, *57*, 4618–4632. [[CrossRef](#)]
20. Yu, Y.; Jiang, L.; Cao, Q.; Xia, B.; Wang, Q.; Lu, Y. Pump-probe imaging of the fs-ps-ns dynamics during femtosecond laser Bessel beam drilling in PMMA. *Opt. Express* **2015**, *23*, 32728–32735. [[CrossRef](#)]
21. Unger, C.; Koch, J.; Overmeyer, L.; Chichkov, B.N. Time-resolved studies of femtosecond-laser induced melt dynamics. *Opt. Express* **2012**, *20*, 24864–24872. [[CrossRef](#)] [[PubMed](#)]
22. Gao, L.; Liang, J.; Li, C.; Wang, L.V. Single-shot compressed ultrafast photography at one hundred billion frames per second. *Nature* **2014**, *516*, 74–77. [[CrossRef](#)] [[PubMed](#)]
23. Liang, J.; Ma, C.; Zhu, L.; Chen, Y.; Gao, L.; Wang, L.V. Single-shot real-time video recording of a photonic Mach cone induced by a scattered light pulse. *Sci. Adv.* **2017**, *3*, e1601814. [[CrossRef](#)] [[PubMed](#)]
24. Jing, J.; Wei, X.; Wang, L.V. Spatio-temporal-spectral imaging of non-repeatable dissipative soliton dynamics. *Nat. Commun.* **2020**, *11*, 2059. [[CrossRef](#)]
25. Fan, L.; Yan, X.; Wang, H.; Wang, L.V. Real-time observation and control of optical chaos. *Sci. Adv.* **2021**, *7*, eabc8448. [[CrossRef](#)]
26. Bioucas-Dias, J.M.; Figueiredo, M.A. A New TwIST: Two-step iterative shrinkage/thresholding algorithms for image restoration. *IEEE Trans. Image Proc.* **2007**, *16*, 2992–3004. [[CrossRef](#)]
27. Guan, Z.; Li, Y.; Wang, F.; Liu, X.; Peng, X.; Xu, T.; Liu, Y. Study on the length of diagnostic time window of CUP-VISAR. *Meas. Sci. Technol.* **2021**, *32*, 125208. [[CrossRef](#)]
28. Dudley, D.; Duncan, W.M.; Slaughter, J. Emerging digital micromirror device (DMD) applications. *Proc. SPIE* **2003**, *4985*, 14–25.
29. Feng, J.; Shin, H.J.; Nasiatka, J.R.; Wan, W.; Young, A.T.; Huang, G.; Comin, A.; Byrd, J.; Padmore, H.A. An X-ray streak camera with high spatiotemporal resolution. *Appl. Phys. Lett.* **2007**, *91*, 134102. [[CrossRef](#)]
30. Eldar, Y.C.; Kutyniok, G. *Compressed Sensing: Theory and Applications*; Cambridge University Press: Cambridge, UK, 2012.
31. Donoho, D.L. Compressed sensing. *IEEE Trans. Inf. Theory* **2006**, *52*, 1289–1306. [[CrossRef](#)]
32. Fruehling, U.; Wieland, M.; Gensch, M.; Gebert, T.; Schuette, B.; Krikunova, M.; Kalms, R.; Budzyn, F.; Grimm, O.; Rossbach, J.; et al. Single-shot terahertz-field-driven X-ray streak camera. *Nat. Photonics* **2009**, *3*, 523–528. [[CrossRef](#)]
33. Erdmann, A.; Fühner, T.; Evanschitzky, P.; Agudelo, V.; Freund, C.; Michalak, P.; Xu, D.B. Optical and EUV projection lithography: A computational view. *Microelectron. Eng.* **2015**, *132*, 21–34. [[CrossRef](#)]
34. Begum, M.; Uddin, M.S. Digital Image Watermarking Techniques: A Review. *Information* **2020**, *11*, 110. [[CrossRef](#)]
35. Wang, Z.; Bovik, A.C.; Sheikh, H.R.; Simoncelli, E.P. Image quality assessment: From error visibility to structural similarity. *IEEE Trans. Image Proc.* **2004**, *13*, 600–612. [[CrossRef](#)] [[PubMed](#)]